



CHORUS

This is the accepted manuscript made available via CHORUS. The article has been published as:

Landau-Zener-Stückelberg-Majorana Interferometry of a Single Hole

Alex Bogan, Sergei Studenikin, Marek Korkusinski, Louis Gaudreau, Piotr Zawadzki, Andy S. Sachrajda, Lisa Tracy, John Reno, and Terry Hargett

Phys. Rev. Lett. **120**, 207701 — Published 18 May 2018

DOI: [10.1103/PhysRevLett.120.207701](https://doi.org/10.1103/PhysRevLett.120.207701)

Landau-Zener-Stückelberg-Majorana interferometry of a single hole

Alex Bogan, Sergei Studenikin,* Marek Korkusinski,

Louis Gaudreau, Piotr Zawadzki, and Andy S. Sachrajda†

Emerging Technology Division, National Research Council, Ottawa, Canada, K1A0R6

Lisa Tracy

Sandia National Laboratories, Albuquerque, New Mexico 87185, USA

John Reno and Terry Hargett

Center for Integrated Nanotechnologies,

Sandia National Laboratories, Albuquerque, New Mexico 87185, USA

(Dated: April 24, 2018)

Abstract

We perform Landau-Zener-Stückelberg-Majorana (LZSM) spectroscopy on a system with strong spin-orbit interaction (SOI), realized as a single hole confined in a gated double quantum dot. Analogous to electron systems, at magnetic field $B = 0$ and high modulation frequencies we observe photon-assisted tunneling (PAT) between dots, which smoothly evolves into the typical LZSM funnel-shaped interference pattern as the frequency is decreased. In contrast to electrons, the SOI enables an additional, efficient spin-flip interdot tunneling channel, introducing a distinct interference pattern at finite B . Magneto-transport spectra at low-frequency LZSM driving show the two channels to be equally coherent. High-frequency LZSM driving reveals complex photon-assisted tunneling pathways, both spin-conserving and spin-flip, which form closed loops at critical magnetic fields. In one such loop an arbitrary hole spin state is inverted, opening the way toward its all-electrical manipulation.

Currently there is interest in coherent control of individual spins in the context of quantum-dot-based quantum computing with spin qubits [1, 2]. In gated devices, single-spin control is achieved with micromagnets [3–5] or nanoantennae [6–8], requiring complex device engineering. Alternative proposals envision rotating the spin of the moving carrier via the electrostatically modulated Rashba spin-orbit interaction (SOI) [9], which promises simpler designs and improved device scalability. In electronic quantum dot systems such electrical spin manipulation has been reported in gated GaAs [10, 11] and InAs devices [12, 13]. However, in these systems the SOI magnitude is small, it is comparable to the strength of nuclear hyperfine interactions, but much smaller than the interdot tunneling coupling [14–17]. On the other hand, theoretical proposals involving holes [18, 19], motivated by predictions of suppressed hyperfine interactions with nuclear spins [20–30], are at very early stages of implementation. In silicon-based hole devices, both lateral [31, 32] and nanowire systems [33, 34], control of the hole spin via the electric dipole spin resonance and the spin Rabi oscillations have been demonstrated [35, 36]. In GaAs-based devices the anisotropies of the hole tunneling current in a magnetic field [37] and the zero in-plane g-factor [38] were traced to the presence of a strong SOI. Signatures of a strong spin-flip tunneling between the dots in a double quantum dot have been detected in magneto-transport [38], but the consequences of strong SOI have not yet been studied at the single-hole level.

In this Letter we use Landau-Zener-Stückelberg-Majorana (LZSM) interferometry to probe the dynamics of a single hole confined in a lateral double-dot device. This experimental technique has been used to study the coherent phenomena in a variety of physical systems [39]. In particular, it was utilized to study the dynamics and to quantify the coherence of electronic charge qubits [40–46] as well as superconducting qubits [47–49]. In gated dots, LZSM interferometry involves applying microwave modulation to the detuning between the dots and measuring the resulting tunnel current or charge configuration. We demonstrate that for a single hole at zero magnetic field the LZSM phenomena arise from a single tunneling channel, analogous to that of the single-electron system. As in electronic samples, we observe the smooth evolution of the discrete photon-assisted tunneling (PAT) pattern at high driving frequencies to characteristic smooth funnel-shaped fringes at low frequencies. An important difference in the spectra occurs in a nonzero magnetic field, where at all driving frequencies we report the coexistence of interference features generated by two tunneling channels: one spin-conserving and one spin-flipping. High-frequency LZSM

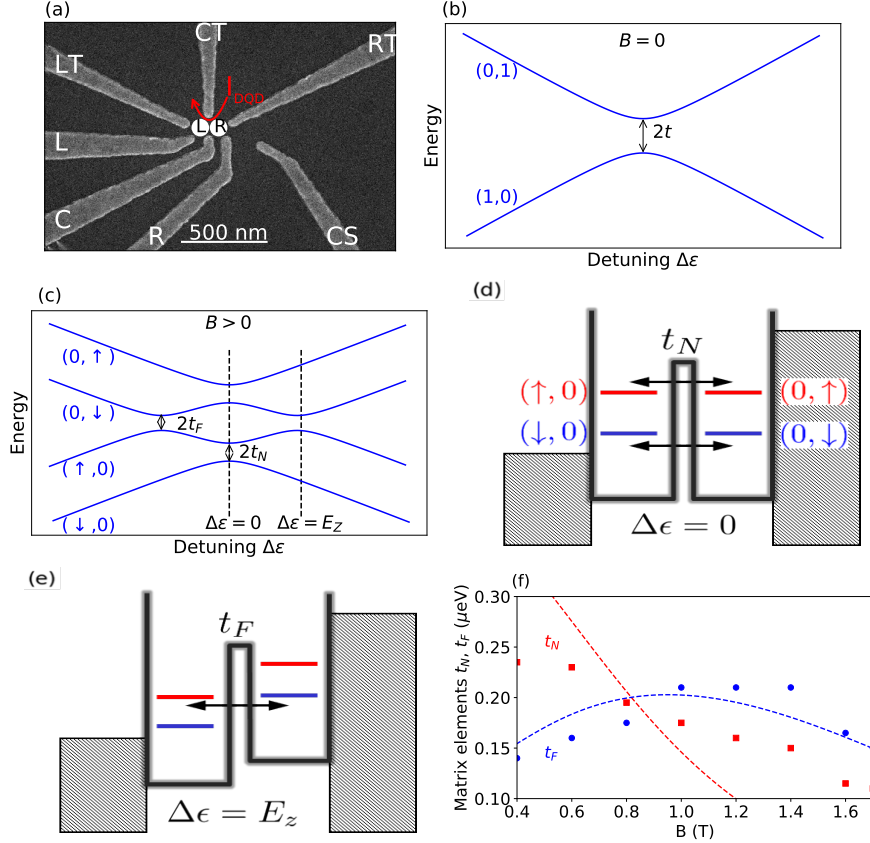


FIG. 1: (a) Layout of the gates forming the double-dot lateral confinement. The red arrow indicates the flow of the current I_{DOT} in the transport measurement. Panels (b) and (c) show the energy diagram of the system as a function of the detuning at zero and nonzero magnetic field, respectively. Panels (d) and (e) show schematic energy diagrams at a nonzero magnetic field, for detunings equal to zero and the Zeeman energy E_Z , respectively. Tunneling matrix elements t_N (t_F) characterize the spin conserving (flipping) tunneling resonance. (f) Magnitudes of the tunneling elements t_N (blue circles) and t_F (red squares) as a function of the magnetic field extracted from experiment (symbols) and predicted by microscopic theory (dashed lines).

interferometry reveals that in systems with strong SOI several microwave-assisted tunneling pathways coexist for optimal values of detuning and magnetic fields, offering novel regimes for new functionalities and means of control of the hybrid charge-spin system.

Figure 1(a) shows the gate layout of our GaAs lateral double dot [38, 50]. We confine precisely one hole and electrically control the charge state between $(n_L, n_R) = (1, 0)$ and $(0, 1)$, where $n_{L(R)}$ is the number of holes in the left-hand (right-hand) dot. A hole can be

placed in each dot in two spin states, which results in four possible combined spin and charge configurations: $(\downarrow, 0)$, $(\uparrow, 0)$, $(0, \downarrow)$, and $(0, \uparrow)$. At zero magnetic field the two spinors in each dot are degenerate. Denoting the energies of $(1, 0)$ and $(0, 1)$ charge configurations by ε_L and ε_R , respectively, the relative detuning $\Delta\varepsilon = \varepsilon_R - \varepsilon_L$ can be tuned by adjusting the voltage on the gate L. Figure 1(b) shows the energy diagram of the system as a function of $\Delta\varepsilon$ at zero magnetic field. It consists of two degenerate energy levels, which anticross close to the resonance, i.e., when $\Delta\varepsilon$ approaches zero, with a gap defined by the interdot tunneling matrix element t . This diagram is identical to that of an equivalent double-dot with a single electron [40–46]. A qualitatively different situation occurs at a finite magnetic field (Fig. 1(c)). Here, the different spin states of the same charge configuration are separated by the Zeeman energy E_Z . States with the same spin exhibit anticrossings at $\Delta\varepsilon = 0$, similar to the electron case, with the gaps defined by the spin-conserving tunneling matrix element t_N . The alignment of dot levels corresponding to that resonance condition is visualized in Fig. 1(d), in which the spin-down (up) levels are represented with blue (red) lines. In our hole system, the strong SOI enables two additional anticrossings between states with opposite spin, with gaps defined by the spin-flip tunneling matrix element t_F . The microscopic form of this SOI component [18, 19, 51, 52] is established in Ref. [53]. The alignment of levels occurring at $\Delta\varepsilon = E_Z$ is shown schematically in Fig. 1(e). Here the left-dot spin-up level $(\uparrow, 0)$ is resonant with the right-dot spin-down level $(0, \downarrow)$ allowing coherent spin-flip tunneling.

Following Refs. [37, 51, 52], we describe our four-level system with a perturbative heavy-hole Hamiltonian in the presence of a magnetic field perpendicular to the dot surface:

$$\hat{H} = \begin{bmatrix} \varepsilon_L + E_Z/2 & 0 & -t_N & -it_F \\ 0 & \varepsilon_L - E_Z/2 & -it_F & -t_N \\ -t_N & it_F & \varepsilon_R + E_Z/2 & 0 \\ it_F & -t_N & 0 & \varepsilon_R - E_Z/2 \end{bmatrix}. \quad (1)$$

The Zeeman energy $E_Z = g^* \mu_B B$, where g^* is the effective hole g-factor [38] (in our system, $g^* = 1.35$), μ_B is the Bohr magneton, and B is the magnetic field. We have estimated the numerical values of the above Hamiltonian elements in magneto-transport spectroscopy by measuring the tunneling current, depicted in Fig. 1(a) with the red arrow, as a function of the detuning $\Delta\varepsilon$ and the magnetic field. We chose a high source-drain bias voltage, corresponding to the alignment of the lead Fermi energies as depicted in Fig. 1(d), (e).

Following the procedure outlined in the supplementary material, Ref. [53], and as shown in Fig. 1(f), the dependence of t_N and t_F on the magnetic field is extracted (red squares and blue dots, respectively). We compare it qualitatively to the trends predicted by a simple microscopic model (red and blue dashed lines, respectively). The spin-flip tunneling element is of a similar magnitude to that of the spin-conserving process, but the two elements differ in their magnetic field dependence. The element t_N decreases, while t_F first increases and then decreases as the field is raised. The behavior of t_N is a consequence of the decreasing overlap between the left and right-dot orbitals due to the diamagnetic tightening of the cyclotron orbits as the field grows. The non-monotonic dependence of t_F , on the other hand, is a direct consequence of the SOI nature of this element, as it depends both on the orbital overlap and the momentum. As the field grows, the overlap between orbitals decreases, but the magnetic vector potential term contributing to the momentum operator grows. The observed behaviour is a result of the interplay of these two trends. A characteristic decrease of the spin-flip tunneling element has been observed for electronic double dots by analyzing the leakage current in the singlet-triplet blockade regime [16].

LZSM interferometry is performed by applying a sinusoidal microwave modulation to gate L . We account for it by replacing the left-dot orbital energy ε_L by $\varepsilon_L + V_0 \sin(2\pi ft)$, where V_0 and f are respectively the modulation amplitude and frequency. To make connection with earlier studies on electronic double-dots [40–46], we first discuss results at zero magnetic field. Figure 2(a) shows the tunneling current as a function of the detuning $\Delta\varepsilon$ and microwave power for a high modulation frequency $f = 15.9$ GHz. Due to the fact that the microwave amplitude delivered to the device depends on the frequency in our setup, we do not calibrate the absolute power levels, but utilize the microwave generator settings in labeling the horizontal axes (the modulation is delivered through a 20 dB attenuator at low temperatures). The set of interference fringes, separated in detuning by hf , corresponds to the equivalent PAT pattern studied in electronic devices, with characteristic modulations in intensity as a function of power. The pattern is reproduced theoretically in Fig. 2(b) by calculating the time-averaged current in the density-matrix rate equation approach [39, 53–55] applied to our four-level model. As the microwave frequency is reduced to 6.7 GHz, the spacing of the PAT fringes in detuning decreases as observed in the experiment, Fig. 2(c) and theory, Fig. 2(d). The interference fringes are broadened by decoherence [39] allowing us to extract the value of the charge qubit decoherence time $T_2^* \approx 60$ and 75 ps for $f = 15.9$

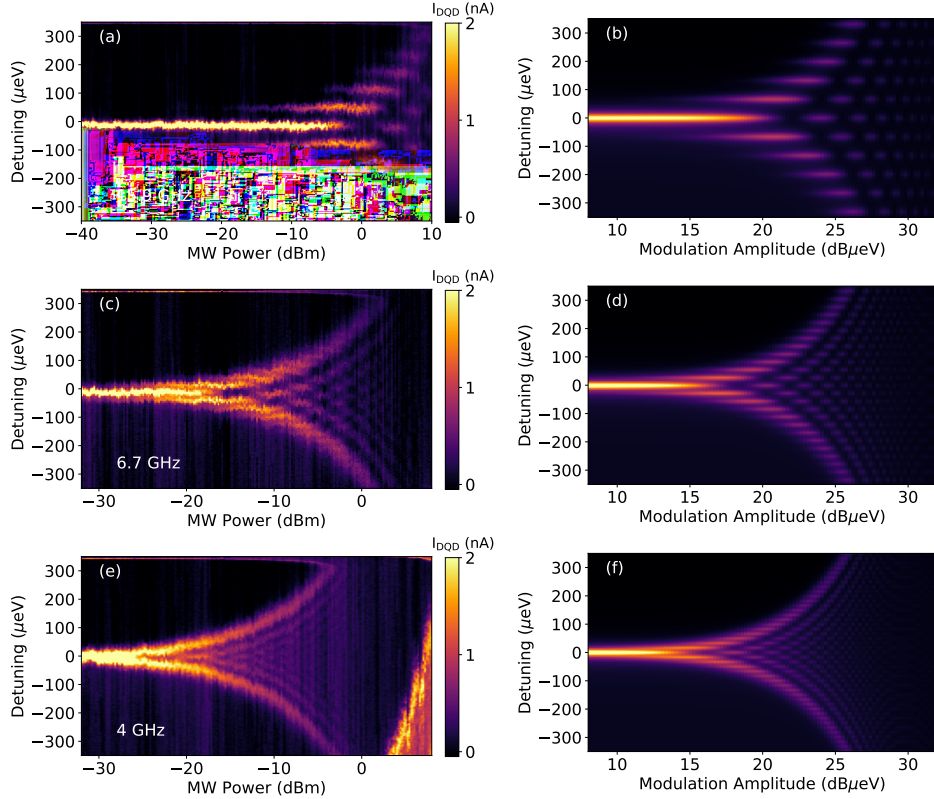


FIG. 2: LZSM interferometry of a single hole at zero magnetic field. Panels (a), (c), and (e) show the tunneling current measured as a function of detuning and microwave power at driving frequencies 15.9 GHz, 6.7 GHz, and 4 GHz, respectively. Panels (b), (d), and (f) show the results of model calculations at matching conditions.

GHz and 6.7 GHz, respectively. For an even lower frequency $f = 4$ GHz [Fig. 2(e) experiment and (f) theory] the fringes coalesce and form funnel-shaped features [56–59]. Here the extracted charge qubit time $T_2^* = 90$ ps.

LZSM spectra are dramatically different in a nonzero magnetic field. Figures 3(a) and (c) show respectively the tunneling current as a function of microwave power for high frequency modulation ($f = 15.9$ GHz) and two values of magnetic field, $B = 1.34$ T and $B = 2.1$ T, respectively. Figure 3(e) shows the current measured at $B = 1$ T and a low-frequency modulation ($f = 2.77$ GHz). Figures 3(b), (d), and (f) show the results of corresponding simulations. Here the spin-conserving and spin-flip tunneling channels become nondegenerate resulting in the appearance of two sets of interference fringes. In Fig. 3(a) we are in the PAT regime. Here the magnetic field was chosen so that the resulting Zeeman energy $E_Z \approx 2hf$, leading to the overlap of first-order interference features of the two patterns.

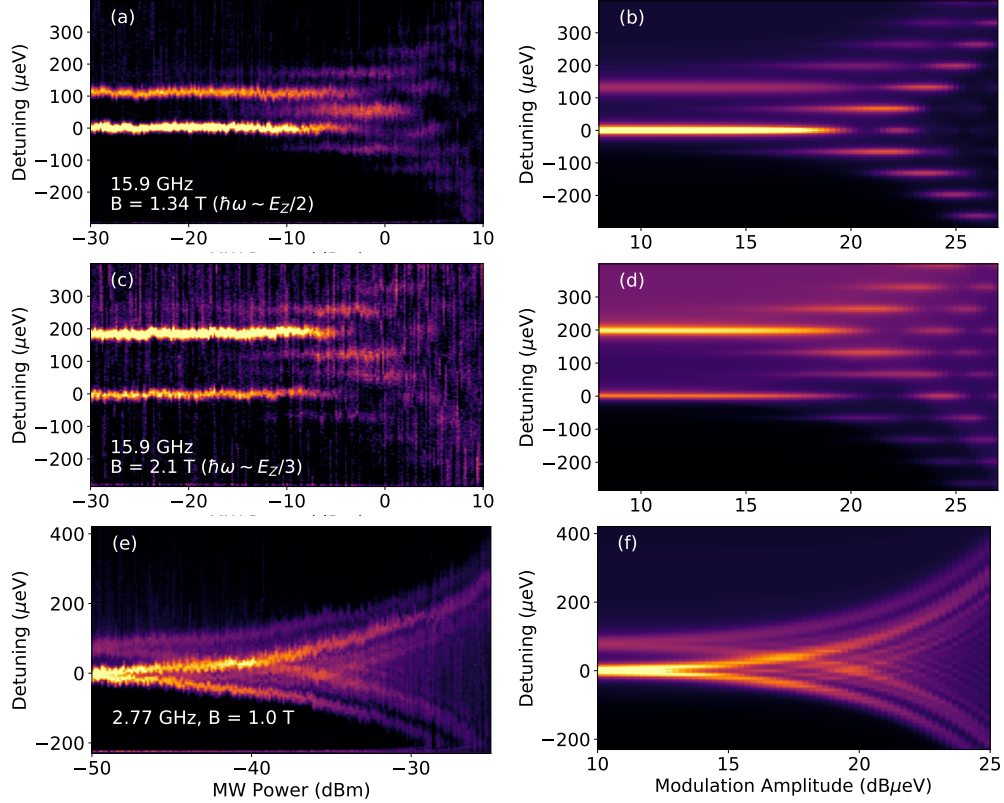


FIG. 3: LZSM interferometry of a single hole at nonzero magnetic fields. Tunneling current measured (a) and calculated (b) as a function of detuning and microwave power for a driving frequency $f = 15.9$ GHz and a magnetic field $B = 1.34$ T. The field is chosen so that the Zeeman energy $E_Z \approx 2hf$. Panels (c) and (d) show the current at $B = 2.1$ T, i.e., $E_Z \approx 3hf$, with the same microwave modulation frequency. Panels (e) and (f) show respectively the tunneling current measured and calculated at $B = 1$ T for a driving frequency $f = 2.77$ GHz.

An increase of the magnetic field to 2.1 T gives the Zeeman energy $E_Z \approx 3hf$, resulting in a relative shift of these patterns in detuning, as seen in Fig. 3(c). In Fig. 3(e) we recover the characteristic low-frequency funnel-shaped fringes at the field of $B = 1$ T. The current maxima evolve from the two-peak structure at low power, through broader, but separate interference patterns at intermediate powers, towards a complex, overlapping structure at high powers. Fitting the LZSM data allows us to extract the tunneling elements t_N and t_F and also the decoherence times T_{2N} and T_{2F} characterizing the spin-conserving and spin-flip tunneling processes, respectively [53]. We find approximately power-independent values of $t_N = 0.26 \pm 0.02 \mu\text{eV}$ and $t_F = 0.28 \pm 0.04 \mu\text{eV}$ at $B = 1$ T. The decoherence times in

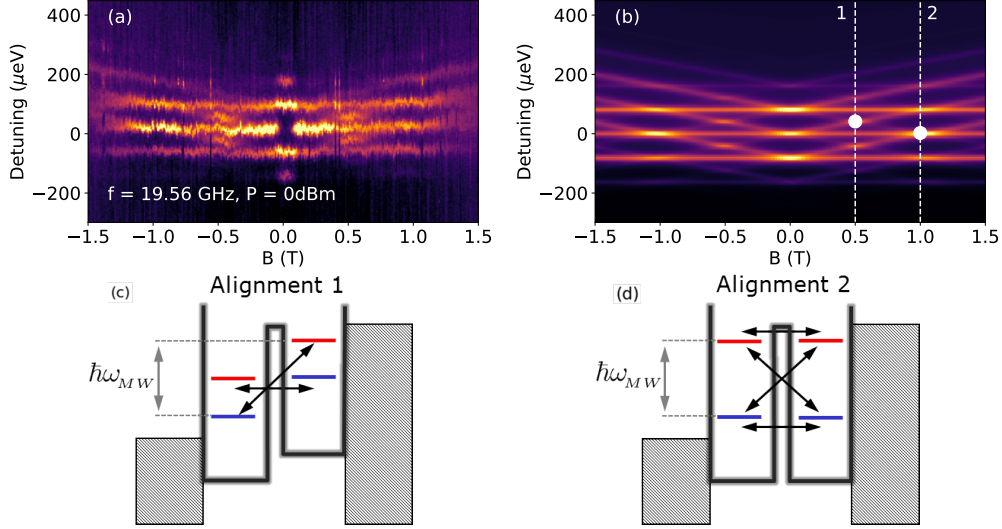


FIG. 4: (a), (b) Measured and calculated tunneling current as a function of detuning (vertical axis) and magnetic field (horizontal axis) at a microwave frequency $f = 19.56$ GHz and power 0 dBm. Panels (c) and (d) show the alignment of quantum dot levels and possible resulting tunneling pathways respectively at conditions (1) and (2) from panel (b).

this spin-charge hybrid regime $T_{2N} \approx T_{2F} = T_2^*$ decrease from ~ 120 ps down to ~ 80 ps as the power increases, which, we speculate, is related to hole heating. The simulation results in Fig. 3 show the current calculated for a power-independent value of $T_2^* = 90$ ps in excellent agreement with the experiment. The existence of the LZSM interference pattern for both tunneling processes indicates that the spin-flip channel is as strong and as coherent as the spin-conserving one. As a result, we deal with a hybrid spin-charge qubit spanned in the basis of four spin-orbital states, with the position and the spin of the hole as orthogonal degrees of freedom. This system differs from the electronic singlet-triplet hybrid qubit demonstrated recently in silicon [60] in that here the tunneling of the hole from one dot to another can be realized both without and with a spin flip, offering enhanced functionality and control.

The relative shift of the two LZSM patterns can be tuned with the magnetic field. To demonstrate this, in Fig. 4(a) we plot the PAT spectra at the microwave power of 5 dBm as a function of the magnetic field, while panel (b) shows the result of simulation. With an excellent agreement between the experiment and theory, we find two clear families of lines. The field-independent (horizontal) features correspond to the spin-conserving transitions, while the field-dependent traces denote the spin-flip resonances. The second family consists

of lines with positive and negative slopes, corresponding to the two spin-flip transitions possible when tunneling from the right to the left dot, i.e., $(0, \uparrow) \rightarrow (\downarrow, 0)$ and $(0, \downarrow) \rightarrow (\uparrow, 0)$. Discrepancies between Fig. 4(a) and (b) at very low magnetic field are most likely due to the aluminum accumulation gate. At low magnetic fields this gate becomes superconducting, which results in a shift of the power level of microwaves delivered to the device, not accounted for in the theoretical model.

Due to their specific magnetic field dependencies, the different families exhibit intersections (degeneracies) at critical values of the field and detuning. In Fig. 4 we indicate two possible types of these intersections. The first one, denoted in panel (b) as (1), involves two fringes, one positively and one negatively sloped in the magnetic field. The diagrammatic description of this condition is shown in panel (c). Since the positions of both fringes are field-dependent, they each correspond to spin-flip tunneling events, albeit at a different PAT order (here, $n = 0$ and $n = +1$) [53]. The resonance condition connects the detuning, Zeeman energy, and microwave frequency via $\Delta\varepsilon = E_Z = hf/2$. Under these conditions, the two independent resonant tunneling channels are enabled simultaneously, and the resultant tunnel current is a simple sum of the two contributions. This is why in Fig. 4(a) and (b) we see a clear enhancement (a bright spot) compared to the visibility of the lines leading into it.

The independence of the two channels makes it possible to invert an arbitrary hole spin state via microwave induced tunneling from the right to the left dot. Indeed, let us prepare the right-dot hole state in the form $\alpha|(0, \uparrow)\rangle + \beta|(0, \downarrow)\rangle$. At this resonance point, the state is transferred (within the LZSM process) to the left-dot state $\beta|(\uparrow, 0)\rangle + \alpha e^{i\phi}|(\downarrow, 0)\rangle$, with a possible phase factor ϕ dependent on the relative phase of the spin-flip and spin-conserving processes. The transfer protocol requires that the effective tunneling elements of order $n = 0$ and $n = 1$ be equal. This can be achieved by controlling the microwave power. Indeed, in the standard PAT treatment such equality is achieved for $J_0(V_0/hf) = J_1(V_0/hf)$, where $J_n(x)$ is the Bessel function of the n -th order [53]. One of the infinitely many solutions of this equation is $V_0 \approx 1.45hf$. Experimental evidence of this equality can be seen in Fig. 3(a) and (c). In the upper (spin-flip) PAT structure, the $n = 0$ and $n = 1$ fringes oscillate out of phase and are equally bright at the microwave power of about -5 dBm. This protocol enables a complete, electrically-controlled hole spin flip, while the control over the phase can be achieved by tuning the Rashba SOI [9]. In our LZSM study we apply a

monochromatic microwave modulation, causing the hole to tunnel back and forth between the dots. However, the hole could be transferred to the left dot in principle by employing appropriate more complex pulse shaping techniques.

The second type of intersection is denoted by the condition (2) in Fig. 4(b), and is visualized schematically in panel (d). At such three-fold intersections, spin-flip and spin-conserving channels of different interference orders are simultaneously active. In this case, $\Delta\varepsilon = 0$ and $E_Z = hf$, resulting in coincidence of $n = \pm 1$ spin-flip and $n = 0$ spin-conserving processes. The four channels depicted in the diagram (d) share common spinors and the process can be seen as a closed loop. One realization of such a loop would begin with placing a hole in the $(0, \downarrow)$ state, from which it could be transferred by the first-order PAT process onto the $(\uparrow, 0)$ state, then by the zero-order tunneling onto the $(0, \uparrow)$ and then onto the $(\downarrow, 0)$ state to end up back in $(0, \downarrow)$. More than one such closed path is possible, e.g., $(0, \downarrow) \rightarrow (\downarrow, 0) \rightarrow (0, \uparrow) \rightarrow (\uparrow, 0) \rightarrow (0, \downarrow)$.

In summary, we have applied LZSM interferometry to study the coherent tunneling of a single hole between the dots of a gated lateral double-dot device. In a transport experiment at zero magnetic field we reproduced the interference patterns recently observed in electronic systems, both at high and low driving frequencies. At finite magnetic fields we demonstrated the coexistence of two, equally strong and equally coherent tunneling channels - one spin-conserving and one spin-flipping, the latter enabled by the strong SOI in the hole system. The resulting formation and coincidence of different photon-assisted tunneling pathways was studied in high-frequency LZSM interferometry. One such coincidence enables a complete inversion (flip) of an arbitrary spin state of the hole as it tunnels between the dots. At the other, more complex resonance point the hole quantum trajectory visits the spin up and down orbitals of the left and right dots in a closed loop. These new features of this LZSM interferometry suggest that novel functionalities can be achieved in a system with strong spin-orbit interaction, opening the way for future experimental studies and applications.

Acknowledgment. AB and SS thanks the Natural Sciences and Engineering Research Council of Canada for financial support. This work was performed in part at the Center for Integrated Nanotechnologies, a U.S. DOE, Office of Basic Energy Sciences user facility, and Sandia National Laboratories, a multi-mission laboratory managed and operated by National Technology and Engineering Solutions of Sandia, LLC., a wholly owned subsidiary of Honeywell International, Inc., for the U.S. Department of Energy's National Nuclear

* Corresponding author, email: sergei.studenikin@nrc.ca

† Corresponding author, email: andy.sachrajda@nrc.ca

- [1] M. A. Nielsen and I. L. Chuang, *Quantum Computation and Quantum Information*, Cambridge University Press, Cambridge, UK, 2010.
- [2] *Semiconductor Quantum Bits*, F. Henneberger and O. Benson (Eds.), Pan Stanford Publishing, Singapore, 2009.
- [3] J. Yoneda, T. Otsuka, T. Takakura, M. Pioro-Ladriere, R. Brunner, H. Lu, T. Nakajima, T. Obata, A. Noiri, C. J. Palmstroem, A. C. Gossard, and S. Tarucha, *Appl. Phys. Express* **8**, 084401 (2015).
- [4] E. A. Laird, C. Barthel, E. I. Rashba, C. M. Marcus, M. P. Hanson, and A. C. Gossard, *Semicond. Sci. Technol.* **24**, 064004 (2009).
- [5] F. Forster, M. Muhlbacher, D. Schuh, W. Wegscheider, and S. Ludwig, *Phys. Rev. B* **91**, 195417 (2015).
- [6] F. H. L. Koppens, C. Buizert, K. J. Tielrooij, I. T. Vink, K. C. Nowack, T. Meunier, L. P. Kouwenhoven, and L. M. K. Vandersypen, *Nature* **442**, 766 (2006).
- [7] F. H. L. Koppens, K. C. Nowack, and L. M. K. Vandersypen, *Phys. Rev. Lett.* **100**, 236802 (2008).
- [8] M. Veldhorst, J. C. C. Hwang, C. H. Yang, A. W. Leenstra, B. de Ronde, J. P. Dehollain, J. T. Muhonen, F. E. Hudson, K. M. Itoh, A. Morello, and A. S. Dzurak, *Nature Nanotechnol.* **9**, 981 (2014).
- [9] S. Datta and B. Das, *Appl. Phys. Lett.* **56**, 665 (1990).
- [10] L. R. Schreiber, F. R. Braakman, T. Meunier, V. Calado, J. Danon, J. M. Taylor, W. Wegscheider, and L. M. K. Vandersypen, *Nature Comm.* **2**, 556 (2011).
- [11] K. C. Nowack, F. H. L. Koppens, Yu. V. Nazarov, and L. M. K. Vandersypen, *Science* **318**, 1430 (2007).
- [12] S. Nadj-Perge, S. M. Frolov, E. P. A. M. Bakkers, and L. P. Kouwenhoven, *Nature* **468**, 1084 (2010).
- [13] A. Pfund, I. Shorubalko, K. Ensslin, and R. Leturcq, *Phys. Rev. B* **76**, 161308(R) (2007).

- [14] J. M. Nichol, S. P. Harvey, M. D. Shulman, A. Pal, V. Umansky, E. I. Rashba, B. I. Halperin, and A. Yacoby, *Nature Comm.* **6**, 7682 (2015).
- [15] S. Nadj-Perge, S. M. Frolov, J. W. W. van Tilburg, J. Danon, Yu. V. Nazarov, R. Algra, E. P. A. M. Bakkers, and L. P. Kouwenhoven, *Phys. Rev. B* **81**, 201305(R) (2010).
- [16] T. Fujita, P. Stano, G. Allison, K. Morimoto, Y. Sato, M. Larsson, J.-H. Park, A. Ludwig, A. D. Wieck, A. Oiwa, and S. Tarucha, *Phys. Rev. Lett.* **117**, 206802 (2016).
- [17] V. F. Maisi, A. Hofmann, M. Roosli, J. Basset, C. Reichl, W. Wegscheider, T. Ihn, and K. Ensslin, *Phys. Rev. Lett.* **116**, 136803 (2016).
- [18] P. Szumniak, S. Bednarek, B. Partoens, and F. M. Peeters, *Phys. Rev. Lett.* **109**, 107201 (2012).
- [19] P. Szumniak, S. Bednarek, J. Pawlowski, and B. Partoens, *Phys. Rev. B* **87**, 195307 (2013).
- [20] X. J. Wang, S. Chesi, and W. A. Coish, *Phys. Rev. Lett.* **109**, 237601 (2012).
- [21] Jan Fischer, W. A. Coish, D. V. Bulaev, and D. Loss, *Phys. Rev. B* **78**, 155329 (2008).
- [22] G. Burkard, *Nature Mater.* **7**, 100 (2008).
- [23] J. Fisher and D. Loss, *Phys. Rev. Lett.* **105**, 266603 (2010).
- [24] A. Tartakovskii, *Nature Photon.* **5**, 647 (2011).
- [25] D. Heiss, S. Schaeck, H. Huebl, M. Bichler, G. Abstreiter, J. J. Finley, D. V. Bulaev, and D. Loss, *Phys. Rev. B* **76**, 241306(R) (2007).
- [26] B. D. Gerardot, D. Brunner, P.A. Dalgarno, P. Ohberg, S. Seidl, M. Kroner, K. Karrai, N. G. Stoltz, P. M. Petroff, and R. J. Warburton, *Nature (London)* **451**, 441 (2008).
- [27] D. Brunner, B.D. Gerardot, P. A. Dalgarno, G. Wust, K. Karrai, N. G. Stoltz, P. M. Petroff, and R. J. Warburton, *Science* **325**, 70 (2009).
- [28] F. Fras, B. Eble, B. Siarry, F. Bernardot, A. Miard, A. Lemaitre, C. Testelin, and M. Chamarro, *Phys. Rev. B* **86**, 161303(R) (2012).
- [29] S. Varwig, A. Rene, A. Greilich, D. R. Yakovlev, D. Reuter, A. D. Wieck, and M. Bayer, *Phys. Rev. B* **87**, 115307 (2013).
- [30] K. De Greve, P. L. McMahon, D. Press, T. D. Ladd, Dirk Bisping, C. Schneider, M. Kamp, L. Worschech, S. Hofling, A. Forchel, and Y. Yamamoto, *Nature Phys.* **7**, 872 (2011).
- [31] R. Li, F. E. Hudson, A. S. Dzurak, and A. R. Hamilton, *Nano Lett.* **15**, 7314 (2015).
- [32] H. Bohuslavskiy, D. Kotekar-Patil, R. Maurand, A. Corna, S. Barraud, L. Bourdet, L. Hutin, Y.-M. Niquet, X. Jehl, S. De Franceschi, M. Vinet, and M. Sanquer, *Appl. Phys. Lett.* **109**,

- 193101 (2016).
- [33] F. A. Zwanenburg, C. E. W. M. van Rijmenam, Y. Fang, C. M. Lieber, and L. P. Kouwenhoven, *Nano Lett.* **9**, 1071 (2009).
 - [34] A. P. Higginbotham, T. W. Larsen, J. Yao, H. Yan, C. M. Lieber, C. M. Marcus, and F. Kuemmeth, *Nano Lett.* **14**, 3582 (2014).
 - [35] B. Voisin, R. Maurand, S. Barraud, M. Vinet, X. Jehl, M. Sanquer, J. Renard, and S. De Franceschi, *Nano Lett.* **16**, 88 (2016).
 - [36] R. Maurand, X. Jehl, D. Kotekar-Patil, A. Corna, H. Bohuslavskyi, R. Lavieville, L. Hutin, S. Barraud, M. Vinet, M. Sanquer, and S. De Franceschi, *Nature Comm.* **7**, 13575 (2016).
 - [37] D. Q. Wang, O. Klochan, J.-T. Hung, D. Culcer, I. Farrer, D. A. Ritchie, and A. R. Hamilton, *Nano Lett.* **16**, 7685 (2016).
 - [38] A. Bogan, S. A. Studenikin, M. Korkusinski, G. C. Aers, L. Gaudreau, P. Zawadzki, A. S. Sachrajda, L. A. Tracy, J. L. Reno, and T. W. Hargett, *Phys. Rev. Lett.* **118**, 167701 (2017).
 - [39] S. N. Shevchenko, S. Ashhab, and F. Nori, *Phys. Reports* **492**, 1 (2010).
 - [40] T. H. Oosterkamp, T. Fujisawa, W. G. van der Wiel, K. Ishibashi, R. V. Hijman, S. Tarucha, and L. P. Kouwenhoven, *Nature* **395**, 873 (1998).
 - [41] L. R. Schreiber, F. R. Braakman, T. Meunier, V. Calado, J. Danon, J. M. Taylor, W. Wegscheider, and L. M. K. Vandersypen, *Nature Commun.* **2**, 556 (2011).
 - [42] M. F. Gonzalez-Zalba, S. N. Shevchenko, S. Barraud, J. R. Johansson, A. J. Ferguson, F. Nori, and A. C. Betz, *Nano Lett.* **16**, 1614 (2016).
 - [43] J. Stehlik, Y. Dovzhenko, J. R. Petta, J. R. Johansson, F. Nori, H. Lu, and A. C. Gossard, *Phys. Rev. B* **86**, 121303(R) (2012).
 - [44] F. Forster, G. Petersen, S. Manus, P. Hanggi, D. Schuh, W. Wegscheider, S. Kohler, and S. Ludwig, *Phys. Rev. Lett.* **112**, 116803 (2014).
 - [45] J. R. Petta, A. C. Johnson, C. M. Marcus, M. P. Hanson, and A. C. Gossard, *Phys. Rev. Lett.* **93**, 186802 (2004).
 - [46] F. R. Braakman, J. Danon, L. R. Schreiber, W. Wegscheider, and L. M. K. Vandersypen, *Phys. Rev. B* **89**, 075417 (2014).
 - [47] W. D. Oliver, Y. Yu, J. C. Le, K. K. Berggren, L. S. Levitov, and T. P. Orlando, *Science* **310**, 1653 (2005).
 - [48] D. M. Berns, M. S. Rudner, S. O. Valenzuela, K. K. Berggren, W. D. Oliver, L.S. Levitov,

- and T. P. Orlando, *Nature* **455**, 51 (2008).
- [49] W. D. Oliver and S. O. Valenzuela, *Quantum Inf. Process.* **8**, 261 (2009).
- [50] L. A. Tracy, T. W. Hargett, and J. L. Reno, *Appl. Phys. Lett.* **104**, 123101 (2014).
- [51] D. Bulaev and D. Loss, *Phys. Rev. Lett.* **98**, 097202 (2007).
- [52] D. Bulaev and D. Loss, *Phys. Rev. Lett.* **95**, 076805 (2005).
- [53] See Supplemental Material at <http://> for the description of the sample and a detailed presentation of the theoretical model, which includes Refs. [61 - 68].
- [54] G. Platero and R. Aguado, *Phys. Reports* **395**, 1 (2004).
- [55] J. Villavicencio, I. Maldonado, E. Cota, and G. Platero, *Phys. Rev. B* **88**, 245305 (2013).
- [56] J. R. Petta, H. Lu, and A. C. Gossard, *Science* **327**, 669 (2007).
- [57] S. A. Studenikin, G. C. Aers, G. Granger, L. Gaudreau, A. Kam, P. Zawadzki, Z. R. Wasilewski, and A. S. Sachrajda, *Phys. Rev. Lett.* **108**, 226802 (2012).
- [58] G. Poulin-Lamarre, J. Thorgrimson, S. A. Studenikin, G. C. Aers, A. Kam, P. Zawadzki, Z. R. Wasilewski, and A. S. Sachrajda, *Phys. Rev. B* **91**, 125417 (2015).
- [59] M. Korkusinski, S. A. Studenikin, G. Aers, G. Granger, A. Kam, and A. S. Sachrajda, *Phys. Rev. Lett.* **118**, 067701 (2017).
- [60] Z. Shi, C. B. Simmons, J. R. Prance, J. K. Gamble, T. S. Koh, Y.-P. Shim, X. Hu, D. E. Savage, M. G. Lagally, M. A. Eriksson, M. Friesen, and S. N. Coppersmith, *Phys. Rev. Lett.* **108**, 140503 (2012).
- [61] Y. Komijani, T. Choi, F. Nichele, K. Ensslin, T. Ihn, D. Reuter, and A. D. Wieck, *Phys. Rev. B* **88**, 035417 (2013).
- [62] L. A. Tracy, J. L. Reno, and T. W. Hargett, LANL Report (2015).
- [63] S. I. Dorozhkin, *Solid State Commun.* **72**, 211-214 (1989).
- [64] R. Winkler, S. J. Papadakis, E. P. De Poortere, and M. Shayegan, *Phys. Rev. Lett.* **85**, 4574 (2000).
- [65] I. Puerto Gimenez, M. Korkusinski, and P. Hawrylak, *Phys. Rev. B* **76**, 075336 (2007).
- [66] O. N. Jouravlev and Yu. V. Nazarov, *Phys. Rev. Lett.* **96**, 176804 (2006).
- [67] F. Gallego-Marcos, R. Sanchez, and G. Platero, *J. Appl. Phys.* **117**, 112808 (2015).
- [68] L. Jacak, P. Hawrylak, and A. Wojs, *Quantum dots*, Springer, Berlin, 1998.